

See discussions, stats, and author profiles for this publication at: <https://www.researchgate.net/publication/231705815>

Stimuli-Responsive Nanoparticles Based on Interaction of Metallacarborane with Poly(ethylene oxide)

ARTICLE in MACROMOLECULES · JULY 2009

Impact Factor: 5.8 · DOI: 10.1021/ma900484y

CITATIONS

20

READS

22

9 AUTHORS, INCLUDING:



Pavel Matejicek

Charles University in Prague

46 PUBLICATIONS 516 CITATIONS

[SEE PROFILE](#)



Jirí Zedník

Charles University in Prague

41 PUBLICATIONS 410 CITATIONS

[SEE PROFILE](#)



Antti Nykänen

National Institute of Metrology, Quality and ...

45 PUBLICATIONS 1,528 CITATIONS

[SEE PROFILE](#)



Janne Ruokolainen

Aalto University

216 PUBLICATIONS 6,603 CITATIONS

[SEE PROFILE](#)

Stimuli-Responsive Nanoparticles Based on Interaction of Metallacarborane with Poly(ethylene oxide)

Pavel Matějček,^{*,†} Jirí Zedník,[†] Katerina Ušelová,[†] Josef Pleštík,[‡] Jindřich Fanfrlík,[§] Antti Nykänen,^{||} Janne Ruokolainen,^{||} Pavel Hobza,[§] and Karel Procházka[†]

[†]Department of Physical and Macromolecular Chemistry, Faculty of Science, Charles University, Hlavova 2030, 128 40 Prague 2, Czech Republic, [‡]Institute of Macromolecular Chemistry, Academy of Sciences of the Czech Republic, Heyrovský Sq. 2, 16206 Prague 6, Czech Republic, [§]Institute of Organic Chemistry and Biochemistry, Center for Biomolecules and Complex Molecular Systems, Gilead Sciences and IOCB Research Center, AS CR, Flemingovo n. 2, 166 10 Prague 6, Czech Republic, and ^{||}Department of Engineering Physics, Helsinki University of Technology, Nanotalo, Puumiehenkuja 2, FI-02150 Espoo, Finland

Received March 5, 2009; Revised Manuscript Received April 2, 2009

ABSTRACT: We report the first evidence that the antiviral active (inhibitor of HIV protease) boron cluster [3-cobalt bis(1,2-dicarbollide)]⁻ anion, CoD⁻, interacts and forms a stable complex with one of the most widely used polymeric components of drug delivery systems: poly(ethylene oxide), PEO. The metallacarborane/polymer complex is insoluble in aqueous solutions. The amount of the precipitate depends on concentration of alkaline or earth-alkaline cations. The formation of insoluble complex is the result of a combination of several factors. One of the decisive contributions is the formation of dihydrogen bonds between negatively charged hydrogen atoms attached to boron atoms and slightly positively charged H atoms in repeating –CH₂–CH₂–O– units. It is also important that alkaline cations interact with oxygen atoms of PEO. The formation of the insoluble NaCoD/PEO complex can be exploited in design of water-soluble [3-cobalt bis(1,2-dicarbollide)]-containing nanoparticles which could offer applications in medicine. We studied the boron cluster interaction with a well-defined double hydrophilic block copolymer: poly(ethylene oxide)-block-poly(methacrylic acid), PEO–PMA. The interaction leads to a spontaneous formation of core–shell nanoparticles. The insoluble core contains the PEO/CoD⁻ complex, while the polyanionic PMA blocks, which do not interact with the cobaltacarborane, form the pH-responsive micellar shell and stabilize the particles in aqueous media. The nanoparticles were studied by light and X-ray scattering, NMR spectroscopy, electrophoresis, and microscopy techniques like AFM and cryo-TEM. It was found that the cores are not completely frozen in aqueous media. Their composition depends on salt concentration, and the metallacarborane can diffuse from/into the nanoparticle after the salinity change.

Introduction

Boron clusters exhibit structural features and chemical properties which offer numerous applications in different research areas and practical fields.^{1–6} After the abandoned high-energy rocket fuel development⁷ in the 1950s and 1960s, other applications have been designed ranging from boron neutron capture therapy (BNCT)^{2,5,8–18} and radionuclide extraction¹⁹ to high temperature resistant polymers, solid electrolytes, catalysts, etc.^{1,4,20–26} As concerns the use of boron clusters in medicine, they have been mostly studied as carriers for BNCT, where their main role consists in delivering sufficient amounts of boron atoms to tumor tissues. Other biomedical applications based on unique properties of boron clusters were investigated to a much less extent. For example, their strong lipophilicity can be utilized in drug design for the modulation of hydrophobic interactions with other biomolecules. Nevertheless, some boron-containing lipophilic pharmacophores and lipophilic components of biologically active macromolecules have been proposed and tested.^{27,28} The use of carboranes as new types of pharmacophores has been attracting interest of scientists in recent years.²⁹ Typically, the icosahedral carborane cluster has been used as a pharmacophore replacing phenyl rings.³⁰ The high resistance to catabolism,

kinetic inertness to reagents, exceptionally high hydrophobicity, and other unique properties facilitate the application of carborane-based compounds for the treatment of an exceptionally broad variety of biological targets including the inhibition of HIV protease^{31–33} and others.^{30,34–37}

Our main attention is focused on the behavior of metal bis (dicarbollides), specifically on [3-cobalt bis(1,2-dicarbollide)]⁻ and on its interaction with water-soluble polymers. The cobalt bis(dicarbollide) ion, which was first prepared and described by Hawthorne in 1965,³⁸ plays a crucial role among all metallaboranes because it is exceptionally thermally and chemically stable and possesses all important properties of carboranes, which differentiate them from other compounds, such as negative charge delocalized over a large area, low nucleophilic behavior, hydrophobicity, and interesting solution and ion-pairing properties. A review on the rich synthetic chemistry of this ion appeared recently in the literature³⁹ along with reviews on other properties and applications.^{19,40}

The charge and surface area influence the hydrophobic or amphiphilic character of different carboranes, their interactions with receptors, and the transfer through the cell membrane.^{8,30,36} The [3-cobalt bis(1,2-dicarbollide)]⁻ cluster surface is composed of hydridic hydrogen atoms that cannot form classical hydrogen bonds. The CoD⁻ salts are water-soluble, but the anion itself exhibits a distinct amphiphilic character. The cobaltacarborane shows high affinity to positively charged groups of other

*To whom correspondence should be sent: Tel +420221951292; Fax +420224919752; e-mail matej@vivien.natur.cuni.cz.

molecules like amino functionalities^{1,41} and peptides. The boron clusters form so-called dihydrogen bonds⁴² that have been recently studied by quantum mechanics calculations.^{43,44}

In spite of extensive pharmaceutical research on boron cluster-containing conjugates, very little attention has been paid to the behavior of their aqueous solutions. Only recently a few reports appeared describing the strong association tendency of metallacarboranes and their bioconjugates in water^{45–48} and at interfaces between water and immiscible solvents.^{49–51} It is obvious that the formation of carborane aggregates in aqueous media complicates their applications in medicine. One of strategies aimed at the successful utilization of carboranes in medicine consists in preparation of thermodynamically stable water-soluble complexes of boron clusters with other molecules. Some time ago, we started a systematic research in this direction. We have already studied the interaction of carborane conjugates with surfactants.⁴⁶ However, the research aimed at possible formation of stimuli-responsive carborane complexes with biocompatible polymers is more important because it can result in straightforward practical applications in a targeted drug delivery.^{52–55}

In this paper, we study the interactions of cobalt bis(dicarbollide) ion, CoD^- , with high-molar-mass poly(ethylene oxide), PEO, and with poly(ethylene oxide)-block-poly(methacrylic acid), PEO-PMA, diblock copolymer. The PEO/ CoD^- interaction in aqueous media has not been described in the literature until now. However poly(ethylene glycol), PEG, with relatively low degree of polymerization was recognized to be an efficient synergist in extraction of alkaline earth cations by cobalt bis(dicarbollide) into organic solvents, where the PEG chains act as a ligand of the metal cation.¹⁹ In the studied system, the complex formation leads to the precipitation of water-soluble compounds, PEO and CoD^- , which seems to be a disadvantage limiting the applicability of PEO in boron cluster containing systems. We will show that the opposite is true. It opens new opportunities in applications as well as in basic research. The aim of the work is (i) a study of interactions that lead to the formation of the PEO/ CoD^- complex, (ii) a reproducible preparation of stable boron-containing polymeric nanoparticles, and (iii) understanding the principles that control this type of self-assembly.

We used PEO-PMA diblock copolymer because it can be prepared in a sufficient quality. Poly(ethylene oxide) is biocompatible, and it has been widely used in medical applications.^{55–57} Poly(methacrylic acid) is a “well-behaving” weak polyelectrolyte suitable for model studies aimed at the elucidation of basic principles of self-assembly.^{58–64} The replacement of the PMA block by other water-soluble polymer (noninteracting with metallacarboranes) will not significantly modify the behavior of the systems suitable for practical applications.

Experimental Section

Materials. Sodium salt of metallacarborane anion [3-cobalt bis(1,2-dicarbollide)]⁻, CoD^- (see Figure 1), was a kind gift of Dr. Bohumír Gruner and Dr. Jaromír Plešek (Institute of Inorganic Chemistry, Academy of Science of the Czech Republic, Řež near Prague). It was characterized using mass spectrometry and ¹H and ¹¹B NMR spectroscopy and in aqueous solutions by other techniques.⁴⁵ All metallacarborane (NaCoD)-containing mixtures were prepared by a manipulation of stock solution ($c = 0.0242 \text{ M}$) in deionized and filtered water.

The poly(ethylene oxide), PEO, linear polymers were purchased from Fluka. They are characterized as follows: the weight-averaged relative molecular weights of PEO samples were 25.8×10^3 and 41.5×10^3 . The polydispersity of all samples was in the range 1.05–1.15. The poly(ethylene oxide)-block-poly(methacrylic acid), PEO-PMA, block copolymer were purchased from Polymer source, Inc. (Dorval, Quebec, Canada).

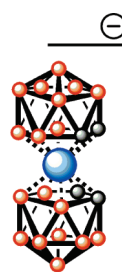


Figure 1. Skeletal structure of the [3-cobalt bis(1,2-dicarbollide)] gauche-rotamer, CoD^- . Color-coding: orange, BH groups; black, CH groups; cyan, cobalt atom.

The weight-averaged relative molecular weights of the PMA and the PEO block, provided by the manufacturer, were 41.0×10^3 and 30.7×10^3 , respectively.

Preparation of Polymeric Complexes. Dialysis tubes with 0.5 mL of aqueous solutions of PEO were placed into a beaker of 0.5 L of dilute NaCoD solution (0.25 mL of 0.0242 M NaCoD stock solution was added to the beaker). To obtain the uptake/release degree of NaCoD by/from the polymer–metallacarborane complexes, the metallacarborane concentration in the bath was monitored by UV-vis spectroscopy at $\lambda = 282 \text{ nm}$. The samples containing the PEO-PMA copolymer were prepared and studied in sodium tetraborate ($\text{Na}_2\text{B}_4\text{O}_10$) buffer ($\text{pH}=9.2$). The dialysis experiments were arranged in such way that equilibration of concentrations in beaker and in water within dialysis tube above the precipitant by diffusion and sorption on the membrane was negligible as compared to the total amount of the PEO/ CoD^- .

Methods. *Infrared Spectroscopy.* Infrared spectra were recorded on a Thermo Nicolet Magna 760 IR instrument equipped with Inspector IR using both undiluted and KBr-diluted samples. The diffuse reflectance technique (DRIFT) (128 or more scans at resolution 4 cm^{-1}) was used.

Dynamic Light Scattering (DLS) and Static Light Scattering (SLS). The light scattering setup (ALV, Langen, Germany) consisted of a 633 nm He-Ne laser, an ALV CGS/8F goniometer, an ALV High QE APD detector, and an ALV 5000/EPP multibit, multitau autocorrelator. DLS data analysis was performed by fitting the measured normalized intensity autocorrelation function $g_2(t) = 1 + \beta|g_1(t)|^2$, where $g_1(t)$ is the electric field correlation function, t is the lag time, and β is a factor accounting for deviation from the ideal correlation. An inverse Laplace transform of $g_1(t)$ with the aid of a constrained regularization algorithm (CONTIN) provides the distribution of relaxation times, $\tau_A(\tau)$. Effective angle- and concentration-dependent hydrodynamic radii, $R_H(q,c)$, were obtained from the mean values of relaxation times, $\tau_m(q,c)$, of individual diffusive modes using the Stokes-Einstein equation. To obtain true hydrodynamic radii, the data have to be extrapolated to a zero scattering angle. The SLS data were treated by the standard Zimm method. The refractive index increments of the NaCoD and PMA-PEO/ CoD^- aqueous solutions obtained by the measurement with the Brice-Phoenix differential refractometer are 0.312 and 0.617 mL/g , respectively.⁶⁵

Atomic Force Microscopy (AFM). AFM measurements were performed in the semicontact (tapping) mode under ambient conditions using a scanning probe microscope NT-MDT NTEGRA Prima equipped with a Nanosensors silicon cantilever. The nanoparticles were deposited from very dilute solutions (ca. 0.01 g/L) on a freshly cleaved mica surface. The samples were left to dry in a vacuum oven.

Cryo-Transmission Electron Microscopy (Cryo-TEM). Glow discharge (Emitech KX100, 2 min/25 mA) treated Quantifoil R2/2 holey carbon copper grid with the hole size of 2 μm was transferred into an environmental chamber of FEI Vitrobot having room temperature and 100% humidity. 3 μL of sample

solution was applied on the grid which was blotted for 1.5 s and then shot to a 1/1 mixture of liquid ethane and propane of temperature -180°C . The grid with vitrified sample film was cryo-transferred into a FEI Tecnai 12 transmission electron microscope with Gatan 910 cryotransfer holder at temperature ca. -185°C . Bright-field TEM was performed using an acceleration voltage of 120 kV, and images were recorded on a Gatan Ultrascan 1000 CCD camera.

Small-Angle X-ray Scattering (SAXS). SAXS experiments were performed using a pinhole camera (Molecular Metrology SAXS System) attached to a microfocused X-ray beam generator (Osmic MicroMax 002) operating at 45 kV and 0.66 mA (30 W). The camera was equipped with a multiwire gas-filled area detector with an active area diameter of 20 cm (Gabriel design). Two experimental setups were used to cover the q range of $0.005\text{--}1.1\text{ \AA}^{-1}$. For a magnitude of the scattering vector, q , stands $q = (4\pi/\lambda) \sin \theta$, where λ is the wavelength and 2θ is the scattering angle. The scattering intensities were put on absolute scale using a glassy carbon standard (details in the Supporting Information).^{66–70}

Capillary Zone Electrophoresis (CZE). The electrophoretic measurements were carried out with ³DCE Instrument (Agilent Technologies, Waldbronn, Germany) with fused silica capillaries (52.8 cm total length, 44.3 cm effective length, 50 μm i.d., 375 μm o.d.; Composite Metal Services, Hallow, UK). The instrument was equipped with a built-in photometric diode array detector (DAD). The separation capillary was thermostated at 25 °C. A separation voltage of +15 kV and a hydrodynamic injection of 120 mbar·s were used in all CZE experiments. Prior to each run, the capillary was flushed 2.5 min with running buffer. The computer program HP ChemStation (Agilent Technologies) was used to data collection and acquisition. The mathematical computer program Origin 8.5 (OriginLab Corp., Northampton, MA) was used for graphical depiction of the results. The background electrolytes contained 2, 10, 30, and 50 mM sodium tetraborate buffer. An aqueous solution of thiourea was used as the electroosmotic flow (EOF) marker. The data were collected at two different λ values: 220 and 280 nm.

¹H NMR Spectroscopy. ¹H and ¹³C{¹H} NMR spectra were measured on a Varian ¹UNITY INOVA 400 in deuterium oxide (99.5%; Chemotrade, Leipzig, Germany). Spectra were referenced to the solvent signal (4.80 ppm). NOESY ¹H NMR experiments were performed using standard three-pulse technique in phase-sensitive mode. Mixing times were 0.1, 0.3, 0.5, and 0.7 s at 25 °C and 0.3 and 0.7 s at 50 °C. ROESY experiments were recorded using a standard pulse sequence with the mixing time set to 0.1 and 0.3 s.

UV–Vis Spectroscopy. UV–vis absorption spectra were carried out with a Hewlett-Packard 8452a diode-array spectrometer.

Results and Discussion

Preparation and Characterization of the Complex of Linear PEO and CoD[−]. In a series of preliminary experiments, we found that NaCoD forms an insoluble complex with PEO in aqueous media. The amount of the precipitate depends strongly on the added salt concentration. For the quantitative study of the complex formation, we performed a set of simple dialysis experiments. A semipermeable tube filled with dilute PEO solution was placed in an excess of NaCoD solution (details in Experimental Section). The changes in the metallacarborane concentration in the external bath were monitored by the UV–vis spectroscopy. The amount of CoD[−] specifically bound to the polymer was recalculated from the decrease in absorbance at $\lambda = 282\text{ nm}$. This decrease is very slow and reaches the equilibrium in times exceeding 300 h (the time dependence is shown in Figure 2). The process is controlled by very slow penetration of bulky CoD[−] anions

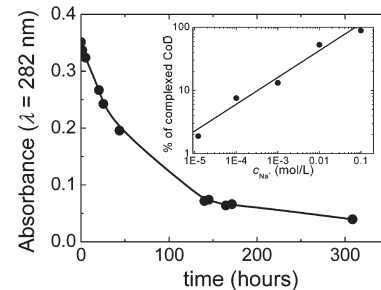


Figure 2. Time dependence of absorbance at 282 nm of a dialysis bath containing 0.25 mL of 0.0242 M NaCoD, 0.1 M NaCl, and a dialysis tube of 0.5 mL of PEO solution (10 g/L) within. Inset: the amount of NaCoD molecules complexed with PEO as a function of NaCl concentration.

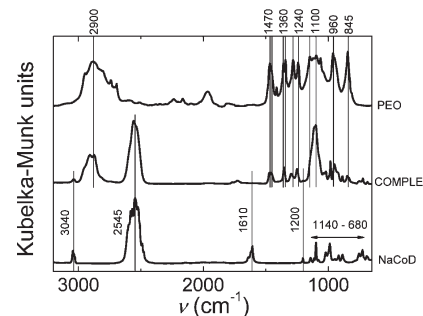


Figure 3. IR spectra of NaCoD (bottom), NaCoD/PEO complex (center), and PEO (top). Interpretation of the bands of PEO: 2900 cm^{-1} $\nu(\text{C}-\text{H})$, 1470 cm^{-1} $\delta(\text{CH}_2)$, 1450 cm^{-1} sr(CH_2), 1360 + 1340 cm^{-1} w(CH_2) + $\nu(\text{C}-\text{C})$, 1280 + 1240 cm^{-1} t(CH_2), 1150 cm^{-1} $\nu(\text{C}-\text{O}-\text{C})$ + $\nu(\text{C}-\text{C})$, 1100 cm^{-1} $\nu(\text{C}-\text{O}-\text{C})$, 960 cm^{-1} r(CH_2), and 845 cm^{-1} r(CH_2). Interpretation of the bands of NaCoD: 3040 cm^{-1} $\nu(\text{C}-\text{H})$, 1610 cm^{-1} crystalline water, 2545 cm^{-1} $\nu(\text{B}-\text{H})$, 1200 cm^{-1} $\delta(\text{C}-\text{H})$, and 1140–680 cm^{-1} skeletal vibrations. Meaning of the symbols: r (rocking), sr (scissoring), t (twisting), w (wagging), δ (bending), and ν (stretching).

through the membrane, since the precipitation in directly mixed solutions is much faster.

The inset in Figure 2 shows the amount of CoD[−] anions incorporated in the complex as a function of NaCl concentration (concentrations of PEO and CoD[−] kept constant). We suppose that the complex composition is probably similar for all NaCl concentrations, and only the amount of the precipitate differs. It is interesting that 1 metallacarborane molecule per ca. 10 of all the PEO monomeric units causes almost quantitative precipitation of the well water-soluble PEO in 0.1 M NaCl. It should be mentioned that the same ratio we got also in 0.05 M sodium tetraborate ($\text{Na}_2\text{B}_4\text{O}_{10}$) buffer, which suggests that only the concentration of Na⁺ plays a role. We carried out dialysis experiments also with 0.1 M solutions of other salts—LiCl, KCl, CsNO₃, MgCl₂, CaCl₂, CuCl₂, and CoCl₂—which were chosen with respect to their practical importance, however without any ambition for completeness. For most salts, we obtained similar results (Figure S1), but we did not study this topic in detail.

The insoluble PEO/cobaltacarborane complex is deeply red colored, sticky, and hygroscopic matter. As mentioned in the Introduction, it has been already reported that PEG (in fact identical to PEO) displays a synergistic effect in the extraction of alkaline earth cations with metal bis (dicarbollide) anions into organic solvents.¹⁹ The effect is explained (see ref 19 and references therein) by an interaction of metal cation with PEG units (confirmed also by

Table 1. Interacting Energies of EO_5/CoD^- , CoD^-/Na^+ , and EO_5/Na^+ Pairs Calculated by Quantum Mechanics Using the C-PCM Implicit Solvent Model^a

interacting pair	EO_5/CoD^-	CoD^-/Na^+	EO_5/Na^+
overall free energy [kcal/mol]	-6.3	15.4	-19.0
"in vacuo" interaction energy [kcal/mol]	-15.8	-92.5	-64.0
desolvation contribution [kcal/mol]	9.6	107.9	45.1

^a Negative values represent the complex formation supporting contributions.

crystallography),^{71,72} which "increases" its solubility in organic media. In water, we expect also an interaction of the boron cluster with polymer chains. Hence, the complex formation proceeds as a solubilization of CoD^- anion in collapsing polymer coils. Significant contribution comes from an electrostatic attraction of bulky and amphiphilic CoD^- ions by cations complexed by PEO chains. These assumptions are in agreement with recently published works on complexation of Na^+ with $-\text{CH}_2-\text{CH}_2-\text{O}-$ linkers covalently bound to boron clusters⁷³ and position of CoD^- counterions in protein structures.⁷⁴

To characterize the precipitant obtained from 0.1 M NaCl solution, we recorded the infrared spectrum of the complex and compared it with spectra of parent compounds. The comparison is shown in Figure 3. The analysis based on literature data^{75–82} leads to the following conclusions: (i) The spectrum contains all characteristic bands of PEO and CoD^- , but it is not a simple superposition of both spectra. (ii) The small band at 3040 cm^{-1} is only little affected by the complex formation, which precludes significant interactions of partially positively charged H atoms (at metallacarborane C atoms) with PEO.⁷⁶ (iii) The mutual PEO and CoD^- interaction is quite weak and do not significantly affect peak positions in the IR spectrum. However narrowing and changes in splitting of several bands (2900 , 1350 , 1100 cm^{-1}) indicates changes in the PEO vibration symmetry. The IR spectroscopy confirms formation of the complex (or better said composite) consisting of both parent compounds due to a weak cooperative binding accompanied by changes in PEO conformation.

To understand the formation of the complex, we carried out quantum mechanics calculations. The cluster of CoD^- , its counterion Na^+ , and the linear pentamer of ethylene oxide EO_5 were studied by the DFT method augmented with an empirical dispersion correction, D .⁸³ We applied the resolution of the identity, RI, approximation⁸⁴ with the TZVP base and the TPSS functional using Turbomole 5.8.⁸⁵ Hydration free energies were calculated using the C-PCM implicit solvent model⁸⁶ implemented in the Gaussian03 code.⁸⁷ The recommended HF/6-31G* level combined with the united atom radii, UAHF, model was used.

Because the $\text{EO}_5/\text{CoD}^-/\text{Na}^+$ complex geometry is very difficult to obtain by the QM calculations, we calculated stabilization energies of all possible interacting pairs. First we focused on the in vacuo contribution as shown in Table 1. The results can be characterized as follows: (i) dihydrogen bonding of boron cluster with EO_5 ($\text{C}-\text{H}^{\delta+}\dots{}^{\delta-}\text{H}-\text{B}$) is relatively weak, (ii) interaction of Na^+ with EO_5 represents a significant contribution, and (iii) interaction energy of Na^+ with CoD^- is strongly attractive which indicates the formation of contact ion pairs in low-permittivity media. It is well-known that the solvation free energy plays important role particularly in aqueous solutions. Therefore, we extended our approach by the C-PCM implicit solvent model to get a more realistic insight. From the values shown in Table 1 it is evident that the desolvation contribution effectively weakens

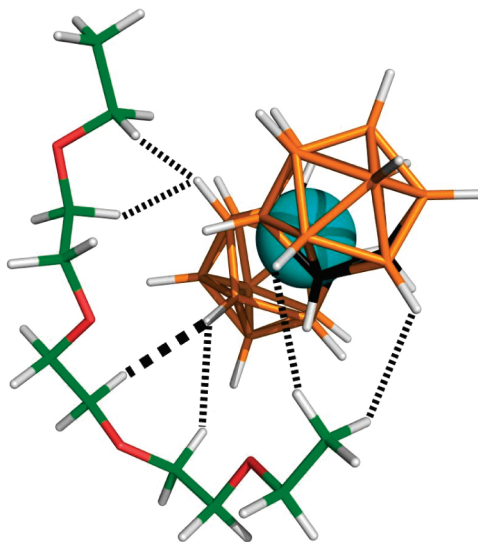


Figure 4. Optimized structure of the metallacarborane and PEO-pentamer complex as a result of quantum mechanics calculations. Possible interactions are depicted. Color coding for metallacarborane: orange, boron; black, carbon; cyan, cobalt; white, hydrogen. Color coding for EO_5 : green, carbon; red, oxygen; white, hydrogen.

the dihydrogen bonding and the EO_5/Na^+ interaction. It also promotes the dissociation of NaCoD , which is a strong electrolyte in aqueous solutions. The implicit solvent model includes the hydrogen bond interaction mediated by water molecules which can furthermore act as bonding partners with the boron cluster via dihydrogen bonds. However, the molecular structure of water around the metallacarborane molecules can be obtained by means of an explicit water model which we are planning to use in our future research. From the results of the C-PCM approximation (Table 1), we can read that the interaction of CoD^- with EO_5 is more favorable than simple dissolution of both components in water. Further, water molecules prefer a mutual interaction via classical hydrogen bonding. On the other hand, the experimental observations indicate that the PEO/ NaCoD composite contains inherent water and behaves as the hydroscopic matter.

Not yet discussed type of interaction which may take place in the studied system is a mutual attraction of boron clusters between each other. In the C-PCM model, a desolvation gain only slightly beats "in vacuo" contribution (electrostatic repulsion of the CoD^- molecules). Hence, a tendency to form complex with EO_5 is favored than a metallacarborane aggregation which is otherwise observed in aqueous solutions.

In the optimized structure of EO_5/CoD^- (shown in Figure 4) there are depicted several dihydrogen bonds, where only one of them is in its optimal geometry (emphasized bond in Figure 4). The other bonds slightly exceed the standard length range of dihydrogen bonds (1.8–2.3 Å). Obviously, CoD^- interacts with poly(ethylene oxide) in the same way as with biomolecules.^{43,44} Therefore, the pair interaction of EO_5/CoD^- seems to be a sufficient driving force for the complex formation. Further, a sum of the individual stabilizing energies obtained using the C-PCM model in Table 1 is negative (first row). However, the calculation shows that an attractive interaction between Na^+ and EO_5 (or PEO) is probably the key precondition of the complex formation (the optimized EO_5/Na^+ structure is shown in Figure S2).

Formation of Nanoparticles Based on Interaction of CoD^- with PEO-PMA. The above-described behavior can be

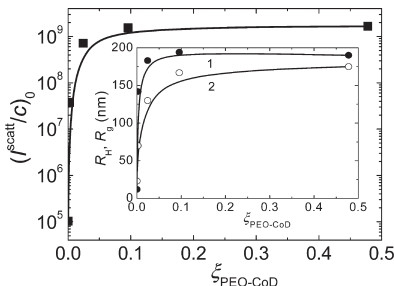


Figure 5. Light scattering intensity extrapolated to zero scattering angle divided by polymer concentration, $(I^{\text{scatt}}/c)_0$, as a function of the $\xi_{\text{PEO-CoD}}$ ratio for PEO-PMA copolymer in 0.05 M sodium tetraborate. Inset: dependence of (curve 1) hydrodynamic radius, R_H , and (curve 2) radius of gyration, R_g , of the PMA-PEO/CoD⁻ particles in 0.05 M sodium tetraborate as a function of the (CoD⁻)-to-PEO units ratio.

exploited in boron-containing drug delivery systems based on double hydrophilic block copolymers. A suitable system for this purpose would be an aqueous dispersion of self-assembled core/shell micelles with insoluble cores containing the PEO/CoD⁻ complex. In this work, we investigated the nanostructures formed by CoD⁻ and poly(ethylene oxide)-block-poly(methacrylic acid) copolymer. The PMA block is not biocompatible, but PEO-PMA can serve as a well-defined model system for studying general behavior of similar systems.^{58–63} The weak polyelectrolyte PMA block is soluble in alkaline buffers in the form of highly charged polyanion which does not form any insoluble complexes with CoD⁻ and stabilizes the nanoparticles in aqueous dispersions. The number of PEO units in PEO-PMA per one NaCoD molecule in 0.05 M sodium tetraborate determined by dialysis was found to be roughly the same as that for linear PEO (ca. 10). We assume that there is no significant difference between a molecular structure of the PEO/CoD⁻ precipitant and the complex dispersed in the form of nanoparticles.

First, we performed the light scattering (LS) measurements of a dilute PEO-PMA solution in 0.05 M borate buffer after the step-by-step addition of the aqueous solution of NaCoD. We expected the formation of micelle-like nanoparticles with the PEO blocks “cross-linked” by the metallacarborane because a similar behavior provoked by multivalent ions or other agents has been observed in case of double hydrophilic polyelectrolytes.^{88–90} The SLS intensity (proportional to the apparent molar mass), hydrodynamic radius (R_H) and radius of gyration (R_g) as functions of the amount of added metallacarborane are shown in Figure 5. The apparent molar mass increases steeply with the addition of CoD⁻ and reaches a plateau at the PEO unit-to-CoD⁻ ratio, $\xi_{\text{PEO-CoD}} = 0.1$ (compare with Figure S1). The solutions contain fairly monodisperse particles, the diameter of which increases in a similar manner like the LS intensity does. The R_g/R_H ratio also increases and reaches the value of ca. 0.85 at high $\xi_{\text{PEO-CoD}}$ values, which can be explained by the fact that the nanoparticles become denser with the addition of CoD⁻. We are aware of the fact that the LS study could be affected by the complicated behavior of CoD⁻ in aqueous solutions. In our previous paper we found that the cobaltacarborane itself forms the self-assembled nanoparticles in aqueous media.⁴⁵ We assume that these aggregates disappear as a result of the interaction of CoD⁻ with the PEO block. Keeping in mind results of QM calculations and a low value of $\xi_{\text{PEO-CoD}}$, the proposed scenario is more realistic than an incorporation of the whole aggregates within polymeric nanostructures.

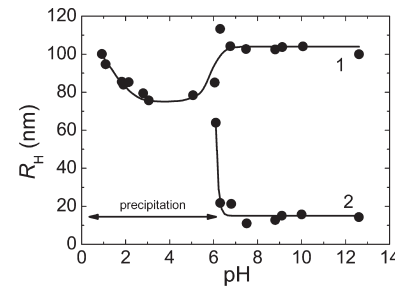


Figure 6. Dependence of the hydrodynamic radius, R_H , of PMA-PEO/CoD⁻ particles in 0.05 M sodium tetraborate with the $\xi_{\text{PEO-CoD}}$ ratio 0.1 (curve 1) and PEO-PMA copolymer in 0.05 M sodium tetraborate (curve 2) as a function of pH.

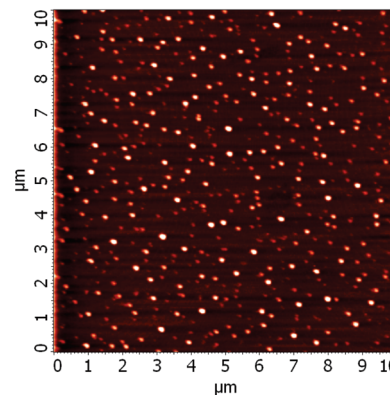


Figure 7. AFM scan of PMA-PEO/CoD⁻ particles with the $\xi_{\text{PEO-CoD}}$ ratio 0.1 prepared by a quick titration and deposited onto mica from basic solution.

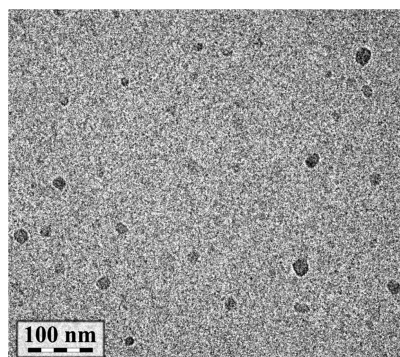


Figure 8. Typical cryo-TEM micrograph of PMA-PEO/CoD⁻ particles with the $\xi_{\text{PEO-CoD}}$ ratio 0.1 in borate buffer ($c = 1 \text{ g/L}$).

The LS data support our assumption that the formed nanoparticles resemble block copolymer micelles.^{59,91} The particles with $\xi_{\text{PEO-CoD}}$ ratio of 0.1 in 0.05 M borate ($\text{Na}_2\text{B}_4\text{O}_{10}$) buffer were characterized by SLS and DLS. The static and dynamic Zimm plots are shown in Figure S3. The unusually high value of dn/dc , ca. 0.6 mL/g, originates from a preferential sorption of CoD⁻ and its counterions within the nanoparticles.^{65,92} From the static Zimm plot, we obtained $R_g = 65.0 \text{ nm}$ and $M_w = 15 \times 10^6 \text{ g/mol}$. As the nanoparticles contain 25% (w/w) of NaCoD the weight average of copolymer aggregation number is 157. The value of R_H obtained from the dynamic Zimm plot is 103.5 nm.

Since we assume the formation of core-shell nanoparticles with the weak polyelectrolyte PMA shells, we studied the

response of particles to pH changes by DLS (see Figure 6). Curve 2 shows the R_H vs pH dependence for pure PEO-PMA chains. The copolymer is molecularly soluble above pH 6 but completely insoluble at low pH.⁶⁴ Curve 1 corresponds to the PMA-PEO/CoD⁻ nanoparticles. The PMA shell shrinks with decreasing pH (in the region below 7).⁵⁹ A sudden increase of the sizes below pH 3 is due to secondary aggregation of nanoparticles as proven by the SLS data (apparent molar mass suddenly increases below pH 3). All these findings were confirmed by AFM (see Figures 7 and S4a,b) after the deposition on a fresh mica surface. Figure 7 shows the nanoparticles prepared and deposited from borate buffer, while in Figure S4a,b we can see the secondary aggregates of individual particles and peculiar wormlike structures deposited from a low pH solution (see also cryo-TEM image in Figure S4c).

The most direct information on the size and shape of nanoparticles in the solution can be obtained by cryo-TEM imaging. A typical micrograph of PMA-PEO/CoD⁻ nanoparticles is shown in Figure 8, where the dark stains correspond to nanoparticle cores, since the shell is invisible due to a low contrast. The morphology of nanoparticles observed by cryo-TEM was compared with the SAXS data as follows. The SAXS scattering curves for the nanoparticles in borate buffer, and the parent samples are shown in Figure S5. Consistent fits of experimental curves (shown in Supporting Information) were obtained only after assumptions that the micellar cores are swollen by bulky CoD⁻ anions. In this case, the SAXS results are comparable with both SLS and cryo-TEM data within experimental errors. The value of the core radius is ca. 18 nm. It is close to the dimensions of the dark stains in Figure 8. Further, the cryo-TEM micrographs visualize PEO/CoD⁻ cores as a uniform matter with no signs of inner domains formed by metallacarborane self-assemblies which otherwise form spontaneously in water.

Because molecular redistribution in polymeric composites is usually slow, it is not surprising that the nanoparticle size depends strongly on the procedure of preparation. The particles prepared by a quick addition of CoD⁻ to a PEO-PMA solution are spherical. They have R_H of ca. 100 nm and aggregation number around 100 (AFM scan shown in Figure 7). These prepared by a step-by-step addition of CoD⁻ have radius of ca. 190 nm with aggregation number reaching several hundred and a tendency to form wormlike structures (Figure S4d,e). The system obtained by an extremely slow dialysis contains polydisperse particles with R_H reaching more than 300 nm consisting of ca. 3000 PEO-PMA chains in average (Figure S4f).

Valuable information on the inner structure of nanoparticles and on the mobility of individual domains can be obtained by ¹H NMR spectroscopy. One important feature of NMR spectra is particularly suitable for our purpose. It is the broadening of signals of nuclei with hindered motion⁹³ which has been widely utilized in polymer research.⁹⁴ A typical ¹H NMR spectrum of PMA-PEO/CoD⁻ alkaline solution in D₂O (Figure S6) contains signals corresponding to the CH₂ group of PEO (1), CH₂ group of PMA (2), and CH₃ group of PMA (3). The signal of CoD⁻ was not observed due to low intensity (concentration) and its incorporation in the rigid complex. We assume no changes in the PMA signals after addition of NaCoD in a well-buffered solution. Hence, the decrease of the relative peak area of PEO can be attributed to the formation of the rigid PEO/CoD⁻ complex. In Figure 9 we can see the fraction of the frozen PEO calculated from the ratio of the peak 1 to the area of all three NMR signals as a function of added CoD⁻. We can conclude that NMR data are consistent with results of

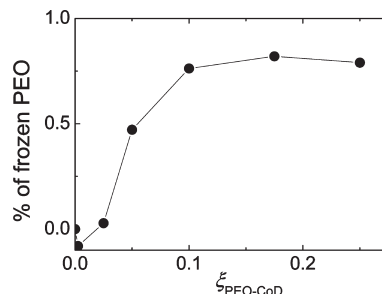


Figure 9. Ratio of frozen PEO units in PMA-PEO/CoD⁻ particles in 0.05 M sodium tetraborate in D₂O as a function of the $\xi_{\text{PEO-CoD}}$ ratio. The values were calculated from corresponding ¹H NMR spectra like in Figure S6.

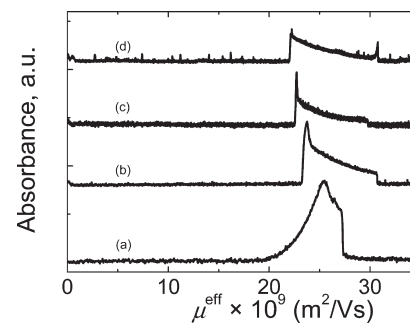


Figure 10. Typical CZE responses of the DAD detector at $\lambda = 280$ nm of the PMA-PEO/CoD⁻ particles with the $\xi_{\text{PEO-CoD}}$ ratio 0.1 in (a) 2, (b) 10, (c) 30, and (d) 50 mM sodium tetraborate running buffers. For a better comparison, the experimental responses were recalculated from a time domain to an electrophoretic mobility domain.

other techniques (LS, dialysis, etc.). The curve shows that ca. 25% of PEO units remain mobile at $\xi_{\text{PEO-CoD}} > 0.1$. They are either unbound PMA-PEO chains or more probably short parts of PEO chains not involved in the complex formation. Further we carried out 2D ¹H NMR experiments—both NOESY and ROESY—because they can reveal possible short-range interactions between PEO and PMA units. As no cross-peaks due to a close contact of PEO and PMA units are present in 2D ¹H NMR spectra, we can conclude that the mobile parts of PEO and PMA are spatially segregated in the nanoparticles.

Remarks on the Dynamic and Stimuli-Responsive Behavior of PMA-PEO/CoD⁻ Nanoparticles. We have already discussed the role of small cations in the process of polymer/metallacarborane complex formation and partially also the response of the system to changes in their concentrations. In this section we summarize results of several techniques used, which allows us to gain a better insight into the dynamic and stimuli-responsive behavior of boron-containing nanoparticles.

The process of PEO/CoD⁻ complex formation was studied by a UV-vis spectroscopy during the dialysis as a function of alkaline or earth-alkaline cations (see the first section in Results and Discussion, especially Figures 2 and S1). Besides the already discussed findings, we noticed that the process is partially reversible and CoD⁻ molecules are released from both PEO/CoD⁻ and PMA-PEO/CoD⁻ complexes by dialysis against pure water. However, the release of CoD⁻ after the drop in $c(\text{Na}^+)$ is very slow. After several weeks of dialysis, only ca. 60% of the bound metallacarborane escapes from the complex into bulk solution.

The salt-induced changes in the complex formation in the PMA-PEO/CoD⁻ system were investigated also by ¹H

NMR spectroscopy in D₂O. The NMR results indicate that the amount of frozen PEO units increases during the addition of sodium chloride due to the penetration of CoD⁻ molecules from the bulk solution into cores of nanoparticles. However, the behavior is more complex. The fraction of frozen PEO surprisingly increases with decreasing $c(\text{Na}^+)$ during dialysis against pure D₂O, despite the fact that we observe a significant CoD⁻ release from nanoparticles by a UV-vis spectroscopy. It means that other mechanisms like the PMA/PEO complex formation⁶² and PEO crystallization⁹⁵ contributing to the PEO immobilization oppose the effect of PEO/CoD⁻ dissociation.

The changes in particle sizes and structure with $c(\text{Na}^+)$ were monitored by LS techniques. The values of R_g , R_H , and apparent M_w were measured in the system containing a constant amount of PEO-PMA and CoD⁻ in 0.005 M borate buffer for a gradually increasing concentration of NaCl up to $c(\text{Na}^+) = 0.2$ M. The value of hydrodynamic radius (around 108 nm) did not almost change (it decreases only very slightly). The radius of gyration grew from 80 to 94 nm. The relative molar mass (ratio of the experimental values of weight-average molar mass for actual and extrapolated to zero salt concentrations, M and M_0 , respectively) is depicted in Figure S7 as a function of $c(\text{Na}^+)$. It appreciably increases with increasing salt concentration. The M/M_0 and R_g/R_H changes with $c(\text{Na}^+)$ reasonably reflect the nanoparticle mass and density increase due to the metallacarborane incorporation in nanoparticles.

The last method we used for studying the dynamic behavior of the complex and the effect of $c(\text{Na}^+)$ on the PMA-PEO/CoD⁻ nanoparticle composition was the capillary zone electrophoresis (CZE). We carried out experiments for the system with $\xi_{\text{PEO}-\text{CoD}} = 0.1$ in the borate buffer as a running electrolyte in a region of concentrations from 2 to 50 mM. We compared the CZE data with results for pure PMA-PEO and NaCoD species in the same buffer. The CZE responses of PMA-PEO/CoD⁻ monitored at the wavelength of 280 nm by the DAD detector (280 nm is the CoD⁻ absorption maximum in water; the polymer is invisible at this wavelength) are shown in Figure 10. In all cases we can see a double-peak pattern which exhibits a peculiar U-shape. This shape is typical for systems with a dynamic equilibrium between two species, and it was described in detail in the literature for CZE^{96–98} as well as other separation techniques (ultracentrifugation, SEC, etc.).⁹⁹ Each component of the system moves with different velocity in the capillary, and the equilibrium is constantly disturbed and reestablished. The left part of peaks in Figure 10 can be assigned to the free metallacarborane, the right part corresponds to the PMA-PEO/CoD⁻ nanoparticles, and the middle part is a result of a gradual release of CoD⁻ from the nanoparticles during the separation process. The CZE measurement also reveals traces of free PEO-PMA chains in the solution. The corresponding peak was detected at $\lambda = 220$ nm in the mobility range higher than the double peak shown in Figure 10. Although the obtained results are only qualitative, the CZE data confirm our assumptions that the nanoparticles are in equilibrium with the metallacarborane and that this equilibrium is strongly affected by $c(\text{Na}^+)$.

Conclusions

Our experimental data unambiguously prove a fairly strong interaction between [3-cobalt bis(1,2-dicarbollide)]⁻ anion and linear poly(ethylene oxide) leading to the formation of an insoluble composite. This not yet described phenomenon is of

high practical importance because both compounds find useful applications in medicine. We performed quantum mechanics calculations which show that boron clusters interact with PEO repeating units via several noncovalent bonds between partially negatively charged hydrogen atoms attached to boron atoms in CoD⁻ and partially positively charged H atoms in CH₂ units of PEO. Besides the formation of dihydrogen bonds, it is also important that cations interact with oxygen atoms of PEO. Hence, the salt concentration is the key factor which can be used for controlling the release in the drug delivery process.

Using a double hydrophilic block copolymer poly(ethylene oxide)-block-poly(methacrylic acid) copolymer and a metallacarborane compound (NaCoD), we prepared a new type of stable self-assembled polymeric core-shell nanoparticles in salted aqueous solutions. Their insoluble cores contain a complex formed by [3-cobalt bis(1,2-dicarbollide)]⁻ anion, poly(ethylene oxide), and small counterions. The nanoparticle dispersions are stabilized by soluble shells formed by weak polyelectrolyte poly(methacrylic acid). Their shape depends on a procedure of preparation and pH of bulk solution, so we can prepare spherical and wormlike micelles or particles with a more complex structure. The study of a fully biocompatible and biodegradable system is planned as the next step of our research. Our forthcoming study should be targeted also on cobalt bis(dicarbollide) conjugates and other types of boron cluster compounds.

Acknowledgment. Authors acknowledge the financial support of the Grant Agency of the Czech Republic (Grants 203/06/P138, 203/06/P261, and 203/05/H001) and the Grant Agency of the Academy of Sciences of the Czech Republic (IAAX00320901). The authors were supported by long-term Research Plan of the Ministry of Education of the Czech Republic No. MSM 0021620857. J.P. gratefully acknowledges the financial support of the Academy of Sciences of the Czech Republic (Project T400500402 in the program "Information Society"), and P.H. and J.F. acknowledge the research Project No. Z40550506. The authors thank Dmitrij V. Bondarev for help with FTIR measurements, Petr Kadlec for the d_n/dc measurements, Zdeněk Tuzar for a fruitful discussion concerning light scattering, and Blanka Vlčková for valuable advice concerning interpretation of IR spectra.

Supporting Information Available: Further experimental details on SAXS, Pedersen and Gerstenberg model and CZE, comments on fitting of the SAXS scattering curves with parameters of the fit, and Figures S1–S7 (dialysis, quantum mechanics, SLS, DLS, AFM, cryo-TEM, SAXS, and NMR characterization). This material is available free of charge via the Internet at <http://pubs.acs.org/>.

References and Notes

- (1) Plesek, J. *Chem. Rev.* **1992**, *92*, 269.
- (2) Valliant, J. F.; Guenther, K. J.; King, A. S.; Morel, P.; Schaffer, P.; Sogbein, O. O.; Stephenson, K. A. *Coord. Chem. Rev.* **2002**, *232*, 173.
- (3) Bregadze, V. I.; Sivaev, I. B.; Glazur, S. A. *Anti-Cancer Agents Med. Chem.* **2006**, *6*, 75.
- (4) Teixidor, F.; Vinas, C.; Demonceau, A.; Nunez, R. *Pure Appl. Chem.* **2003**, *75*, 1305.
- (5) Lesnikowski, Z. J.; Shi, J.; Schinazi, R. F. *J. Organomet. Chem.* **1999**, *581*, 156.
- (6) Grimes, R. N. *J. Chem. Educ.* **2004**, *81*, 658.
- (7) Smith, I. C.; Hughes, R. J.; Lawless, W. H. *Production of Boranes and Related Research*, 1st ed.; Academic Press: New York, 1967.
- (8) Soloway, A. H.; Tjarks, W.; Barnum, B. A.; Rong, F. G.; Barth, R. F.; Codogni, I. M.; Wilson, J. G. *Chem. Rev.* **1998**, *98*, 1515.
- (9) Soloway, A. H.; Barth, R. F.; Gahbauer, R. A.; Blue, T. E.; Goodman, J. H. *J. Neuro-Oncol.* **1997**, *33*, 9.
- (10) Hawthorne, M. F. *Angew. Chem., Int. Ed. Engl.* **1993**, *32*, 950.

- (11) Hawthorne, M. F. *Mol. Med. Today* **1998**, *4*, 174.
- (12) Hawthorne, M. F.; Lee, M. W. *J. Neuro-Oncol.* **2003**, *62*, 33.
- (13) Barth, R. F.; Soloway, A. H.; Goodman, J. H.; Gahbauer, R. A.; Gupta, N.; Blue, T. E.; Yang, W. L.; Tjarks, W. *Neurosurgery* **1999**, *44*, 433.
- (14) Lesnikowski, Z. *J. Curr. Org. Chem.* **2007**, *11*, 355.
- (15) Vitale, A. A.; Hoffmann, G.; Pomilio, A. B. *Mol. Med. Chem.* **2005**, *8*, 1.
- (16) Vicenta, M. G. H. *Anti-Cancer Agents Med. Chem.* **2006**, *6*, 73.
- (17) Adam, M. J.; Wilbur, D. S. *Chem. Soc. Rev.* **2005**, *34*, 153.
- (18) Bregadze, V. I.; Glazun, S. A. *Russ. Chem. Bull., Int. Ed.* **2007**, *56*, 620.
- (19) Rais, J.; Gruner, B. In *Solvent Extraction*; Marcus, I., SenGupta, A. K. Eds.; Marcel Dekker: New York, 2005; p 243.
- (20) Green, J.; Cohen, M. S.; Kotloby, A. P.; Mayes, N.; O'Brien, E. L.; Fein, M. M. *J. Polym. Sci., Part B: Polym. Lett.* **1964**, *2*, 109.
- (21) Fox, M. A.; Wade, K. *J. Mater. Chem.* **2002**, *12*, 1301.
- (22) Wei, X. L.; Carroll, P. J.; Sneddon, L. G. *Chem. Mater.* **2006**, *18*, 1113.
- (23) Jakle, F. *J. Inorg. Organomet. Polym.* **2005**, *15*, 293.
- (24) Simon, Y. C.; Ohm, C.; Zimny, M. J.; Coughlin, E. B. *Macromolecules* **2007**, *40*, 5628.
- (25) Benhabbour, S. R.; Parrott, M. C.; Gratton, S. E. A.; Adronov, A. *Macromolecules* **2007**, *40*, 5678.
- (26) Crespo, E.; Gentil, S.; Vinas, C.; Teixidor, F. *J. Phys. Chem. C* **2007**, *111*, 18381.
- (27) Yamamoto, K.; Endo, Y. *Bioorg. Med. Chem. Lett.* **2001**, *11*, 2389.
- (28) Fujii, S.; Goto, T.; Ohta, K.; Hashimoto, Y.; Suzuki, T.; Ohta, S.; Endo, Y. *J. Med. Chem.* **2005**, *48*, 4654.
- (29) Armstrong, A. F.; Valliant, J. F. *Dalton Trans.* **2007**, *38*, 4240.
- (30) Lesnikowski, Z. *J. Collect. Czech. Chem. Commun.* **2007**, *72*, 1646.
- (31) Cigler, P.; Kozisek, M.; Rezacova, P.; Brynda, J.; Otwinowski, Z.; Pokorna, J.; Plesek, J.; Gruner, B.; Doleckova-Maresova, L.; Masa, M.; Sedlacek, J.; Bodem, J.; Krausslich, H. G.; Kral, V.; Konvalinka, J. *Proc. Natl. Acad. Sci. U.S.A.* **2005**, *102*, 15394.
- (32) Kozisek, M.; Cigler, P.; Lepšík, M.; Fanfrlik, J.; Rezacova, P.; Brynda, J.; Pokorna, J.; Plesek, J.; Gruner, B.; Grantz-Saskova, K.; Vaclavikova, J.; Kral, V.; Konvalinka, J. *J. Med. Chem.* **2008**, *51*, 4839.
- (33) Debnath, A. K.; Jiang, S. B.; Strick, N.; Lin, K.; Kahl, S. B.; Neurath, A. R. *Med. Chem. Res.* **1999**, *9*, 267.
- (34) Tsuji, M.; Koiso, Y.; Takahashi, H.; Hashimoto, Y.; Endo, Y. *Biol. Pharmacol. Bull.* **2000**, *23*, 513.
- (35) Julius, R. L.; Farha, O. K.; Chiang, J.; Perry, L. J.; Hawthorne, M. F. *Proc. Natl. Acad. Sci. U.S.A.* **2007**, *104*, 4808.
- (36) Seidler, J.; McGovern, S. L.; Doman, T. N.; Shoichet, B. K. *J. Med. Chem.* **2003**, *46*, 4486.
- (37) Sibrian-Vazquez, M.; Hao, E.; Jensen, T. J.; Vicente, M. G. H. *Bioconjugate Chem.* **2006**, *17*, 928.
- (38) Hawthorne, M. F.; Young, D. C.; Wegner, P. A. *J. Am. Chem. Soc.* **1965**, *87*, 1818.
- (39) Sivaev, I. B.; Bregadze, V. I. *Collect. Czech. Chem. Commun.* **1999**, *64*, 783.
- (40) Semioshkin, A. A.; Sivaev, I. B.; Bregadze, V. I. *Dalton Trans.* **2008**, *8*, 977.
- (41) Plesek, J.; Base, K.; Mares, F.; Hanousek, F.; Stibr, B.; Hermanek, S. *Collect. Czech. Chem. Commun.* **1984**, *49*, 2776.
- (42) Planas, J. G.; Vinas, C.; Teixidor, F.; Comas-Vives, A.; Ujaque, G.; Lledos, A.; Light, M. E.; Hursthouse, M. B. *J. Am. Chem. Soc.* **2005**, *127*, 15976.
- (43) Fanfrlik, J.; Lepšík, M.; Horinek, D.; Havlas, Z.; Hobza, P. *Chem. Phys. Chem.* **2006**, *7*, 1100.
- (44) Fanfrlik, J.; Hnyk, D.; Lepšík, M.; Hobza, P. *Phys. Chem. Chem. Phys.* **2007**, *9*, 2085.
- (45) Matějček, P.; Cigler, P.; Prochazka, K.; Kral, V. *Langmuir* **2006**, *22*, 575.
- (46) Matějček, P.; Cigler, P.; Olejniczak, A. B.; Andrysiak, A.; Wojtczak, B.; Prochazka, K.; Lesnikowski, Z. *J. Langmuir* **2008**, *24*, 2625.
- (47) Kubat, P.; Lang, K.; Cigler, P.; Kozisek, M.; Matějček, P.; Janda, P.; Zelinger, Z.; Prochazka, K.; Kral, V. *J. Phys. Chem. B* **2007**, *111*, 4539.
- (48) Hao, E.; Sibrian-Vazquez, M.; Serem, W.; Garno, J. C.; Fronczek, F. R.; Vicente, M. G. H. *Chem.—Eur. J.* **2007**, *13*, 9035.
- (49) Chevrot, G.; Schurhammer, R.; Wipff, G. *J. Phys. Chem. B* **2006**, *110*, 9488.
- (50) Chevrot, G.; Schurhammer, R.; Wipff, G. *Phys. Chem. Chem. Phys.* **2007**, *9*, 1991.
- (51) Chevrot, G.; Schurhammer, R.; Wipff, G. *Phys. Chem. Chem. Phys.* **2007**, *9*, 5928.
- (52) Harada, A.; Kataoka, K. *Prog. Polym. Sci.* **2006**, *31*, 949.
- (53) Zhao, Q.; Ni, P. H. *Prog. Chem.* **2006**, *18*, 768.
- (54) Rodriguez-Hernandez, J.; Checot, F.; Gnanou, Y.; Lecommandoux, S. *Prog. Polym. Sci.* **2005**, *30*, 691.
- (55) Gil, E. S.; Hudson, S. A. *Prog. Polym. Sci.* **2004**, *29*, 1173.
- (56) Lavasanifar, A.; Samuel, J.; Kwon, G. S. *Adv. Drug Delivery Rev.* **2002**, *54*, 169.
- (57) Cigler, P.; Kral, V.; Kozisek, M.; Konvalinka, J.; Mirsky, V. M. *Colloids Surf., B* **2008**, *64*, 145.
- (58) Matějček, P.; Uchman, M.; Lokajova, J.; Stepanek, M.; Prochazka, K.; Spirkova, M. *J. Phys. Chem. B* **2007**, *111*, 8394.
- (59) Matějček, P.; Podhajecka, K.; Humpolickova, J.; Uhlik, F.; Jelinek, K.; Limpouchova, Z.; Prochazka, K.; Spirkova, M. *Macromolecules* **2004**, *37*, 10141.
- (60) Uhlik, F.; Limpouchova, Z.; Jelinek, K.; Prochazka, K. *J. Chem. Phys.* **2003**, *118*, 11258.
- (61) Matějček, P.; Uhlik, F.; Limpouchova, Z.; Prochazka, K.; Tuzar, Z.; Webber, S. E. *Macromolecules* **2002**, *35*, 9487.
- (62) Stepanek, M.; Podhajecka, K.; Tesarova, E.; Prochazka, K.; Tuzar, Z.; Brown, W. *Langmuir* **2001**, *17*, 4240.
- (63) Stepanek, M.; Podhajecka, K.; Prochazka, K.; Teng, Y.; Webber, S. E. *Langmuir* **1999**, *15*, 4185.
- (64) Konak, C.; Sedlak, M. *Macromol. Chem. Phys.* **2007**, *208*, 1893.
- (65) The values experimentally determined by Dr. P. Kadlec at IMC, Prague.
- (66) Sommer, C.; Pedersen, J. S.; Stein, P. C. *J. Phys. Chem. B* **2004**, *108*, 6242.
- (67) The value experimentally determined by Dr. A. Sikora at IMC, Prague.
- (68) Plestil, J. *Makromol. Chem., Macromol. Symp.* **1988**, *15*, 185.
- (69) Pedersen, J. S.; Gerstenberg, M. C. *Macromolecules* **1996**, *29*, 1363.
- (70) Plestil, J. *J. Appl. Crystallogr.* **2000**, *33*, 600.
- (71) Henderson, W. A.; Brooks, N. R.; Young, V. G. *J. Am. Chem. Soc.* **2003**, *125*, 12098.
- (72) Lightfoot, P.; Mehta, M. A.; Bruce, P. G. *J. Mater. Chem.* **1992**, *2*, 379.
- (73) Farras, P.; Teixidor, F.; Kivekas, R.; Sillanpaa, R.; Vinas, C.; Gruner, B.; Cisarova, I. *Inorg. Chem.* **2008**, *47*, 9497.
- (74) Fanfrlik, J.; Brynda, J.; Rezac, J.; Hobza, P.; Lepšík, M. *J. Phys. Chem. B* **2008**, *112*, 15094.
- (75) Warren, L. F.; Hawthorne, F. M. *J. Am. Chem. Soc.* **1970**, *92*, 1157.
- (76) Leites, L. A. *Chem. Rev.* **1992**, *92*, 279.
- (77) Vincent, C. A. *Prog. Solid State Chem.* **1987**, *17*, 145.
- (78) Rozenberg, M.; Loewenschuss, A.; Marcus, Y. *Spectrochim. Acta, Part A* **1998**, *54*, 1819.
- (79) Papke, B. L.; Ratner, M. A.; Shriner, D. F. *J. Phys. Chem. Solids* **1981**, *42*, 493.
- (80) Sreekanth, T.; Reddy, M. J.; Ramalingaiah, S.; Rao, U. V. S. *J. Power Sources* **1999**, *79*, 105.
- (81) DiNoto, V.; Bettinelli, M.; Furlani, M.; Lavina, S.; Vidali, M. *Macromol. Chem. Phys.* **1996**, *197*, 375.
- (82) Kumar, J. S.; Kumar, K. V.; Subrahmanyam, A. R.; Reddy, M. J. *J. Mater. Sci.* **2007**, *42*, 5752.
- (83) Jurecka, P.; Cerny, J.; Hobza, P.; Salahub, D. R. *J. Comput. Chem.* **2007**, *28*, 555.
- (84) Feyereisen, M.; Fitzgerald, G.; Komornicki, A. *Chem. Phys. Lett.* **1993**, *208*, 359.
- (85) Ahlrichs, R.; Bar, M.; Haser, M.; Horn, H.; Kolmel, C. *Chem. Phys. Lett.* **1989**, *162*, 165.
- (86) Cossi, M.; Barone, V.; Cammi, R.; Tomasi, J. *Chem. Phys. Lett.* **1996**, *255*, 327.
- (87) Frisch, M. J.; Trucks, G. W.; Schlegel, H. B.; Scuseria, G. E.; Robb, M. A.; Cheeseman, J. R.; Montgomery, J. A., Jr.; Vreven, T.; Kudin, K. N.; Burant, J. C.; Millam, J. M.; Iyengar, S. S.; Tomasi, J.; Barone, V.; Mennucci, B.; Cossi, M.; Scalmani, G.; Rega, N.; Petersson, G. A.; Nakatsuji, H.; Hada, M.; Ehara, M.; Toyota, K.; Fukuda, R.; Hasegawa, J.; Ishida, M.; Nakajima, T.; Honda, Y.; Kitao, O.; Nakai, H.; Klene, M.; Li, X.; Knox, J. E.; Hratchian, H. P.; Cross, J. B.; Adamo, C.; Jaramillo, J.; Gomperts, R.; Stratmann, R. E.; Yazyev, O.; Austin, A. J.; Cammi, R.; Pomelli, C.; Ochterski, J. W.; Ayala, P. Y.; Morokuma, K.; Voth, G. A.; Salvador, P.; Dannenberg, J. J.; Zakrzewski, V. G.; Dapprich, S.; Daniels, A. D.; Strain, M. C.; Farkas, O.; Malick, D. K.; Rabuck, A. D.; Raghavachari, K.; Foresman, J. B.; Ortiz, J. V.; Cui, Q.; Baboul, A. G.; Clifford, S.; Cioslowski, J.; Stefanov, B. B.; Liu, G.; Liashenko, A.;

- Piskorz, P.; Komaromi, I.; Martin, R. L.; Fox, D. J.; Keith, T.; Al-Laham, M. A.; Peng, C. Y.; Nanayakkara, A.; Challacombe, M.; Gill, P. M. W.; Johnson, B.; Chen, W.; Wong, M. W.; Gonzalez, C.; Pople, J. A. *Gaussian03*; Gaussian, Inc.: Pittsburgh, PA, 2003.
- (88) Cohen Stuart, M. A.; Hofs, B.; Voets, I. K.; de Keizer, A. *Curr. Opin. Colloid Interface Sci.* **2005**, *10*, 30.
- (89) Bronich, T. K.; Keifer, P. A.; Shlyakhtenko, L. S.; Kabanov, A. V. *J. Am. Chem. Soc.* **2004**, *127*, 8236.
- (90) Gatsouli, K. D.; Pispas, S.; Kamitsos, E. I. *J. Phys. Chem. C* **2007**, *111*, 15201.
- (91) Zhang, L.; Eisenberg, A. *J. Am. Chem. Soc.* **1996**, *118*, 3168.
- (92) Tuzar, Z.; Kratochvil, P. *Collect. Czech. Chem. Commun.* **1967**, *32*, 3358.
- (93) Cosgrove, T.; Griffiths, P. C. *Adv. Colloid Interface Sci.* **1992**, *42*, 175.
- (94) Kawaguchi, S.; Winnik, M. A.; Ito, K. *Macromolecules* **1996**, *29*, 4465.
- (95) Polik, W. F.; Burchard, W. *Macromolecules* **1983**, *16*, 978.
- (96) Newman, C. I. D.; Collin, G. E. *Electrophoresis* **2008**, *29*, 44.
- (97) Krylov, S. E. *Electrophoresis* **2007**, *28*, 69.
- (98) Trapp, O. *Electrophoresis* **2006**, *27*, 534.
- (99) Prochazka, K.; Mandak, T.; Bednar, B.; Trnena, J.; Tuzar, Z. *J. Liq. Chromatogr.* **1990**, *13*, 1765.

Supporting Information

Stimuli-Responsive Nanoparticles Based on Interaction of Metallacarborane with Poly(ethylene oxide)

Pavel Matějíček,^{*} Jiří Zedník, Kateřina Ušelová, Josef Pleštil, Jindřich Fanfrlík, Antti Nykänen, Janne Ruokolainen, Pavel Hobza, and Karel Procházka

* Department of Physical and Macromolecular Chemistry, Faculty of Science, Charles University, Hlavova 2030, 128 40 Prague 2, Czech Republic
matej@vivien.natur.cuni.cz

Further Experimental Details

Small Angle X-ray Scattering (SAXS). Weight-average of the molar mass of particle was determined from the scattering intensity extrapolated to zero scattering angle corrected for interparticle interference, $I(0)$, as

$$M_w = I(0)N_A / c(\Delta b)^2 \quad (1)$$

where N_A is the Avogadro number and c the particle concentration (g/mL),

$$\Delta b = b - \tilde{V}\rho_0 \quad (2)$$

is the excess scattering length (cm/g), b is the scattering length per one gram of solute (cm/g), \tilde{V} is the partial specific volume of the solute (mL/g) and ρ_0 is the scattering length density of the solvent (cm⁻²). The contrast factors were calculated from Equation 2 using the partial volumes of PEO (0.836 mL/g) [Sommer, C.; Pedersen, J. S.; Stein, P. C. *J. Phys. Chem. B* **2004**, *108*, 6242] and NaCoD (0.714 mL/g) [The value experimentally determined by Dr. A. Sikora at IMC, Prague]. The partial volume of PMA in aqueous media depends strongly on the extent of dissociation. For PMA, we determined Δb directly from the concentration dependence of the integrated SAXS intensity. For this purpose we used a modification of the procedure suggested

earlier [Plestil, J. *Makromol. Chem. Macromol. Symp.* **1988**, *15*, 185]. For increasing concentration of PMA we found the values of Δb ranging from 3.5×10^{10} cm/g at $c < 6$ g/L to 2.1×10^{10} cm/g at $c > 20$ g/L. We used the latter value because we believe that it has been obtained for conditions closer to those for PMA in the associated state.

SAXS: Pedersen and Gerstenberg (P&G) Model [Pedersen, J. S.; Gerstenberg, M. C. *Macromolecules* **1996**, *29*, 1363]: In this model it is assumed that the micelle consists of a spherical core to which corona chains are attached. In the derivation of the scattering function, these chains are assumed to have shapes of statistical polymer coils penetrating freely into the core. Comparison with the results of Monte Carlo simulation showed that the effect of this unrealistic assumption can be compensated by shifting the starting point of the chains from R_{core} to $R_{\text{start}} \equiv R_{\text{core}} + R_{\text{G,chain}}$. In monodisperse case, the relevant model parameters are: aggregation number, N_{agg} , volume per one core-forming block, V_1 , core radius, R_{core} , radius of gyration of the shell-forming chain, $R_{\text{G,chain}}$, the excess scattering amplitudes of the copolymer blocks, ΔB_{core} and ΔB_{chain} , the starting distance, R_{start} , and the number density of the micelles, n . For polydisperse case, we expressed the aggregation number through the micelle core radius, R . The Schulz-Zimm formula was used for the distribution of the radii. The appropriately modified scattering function is given in Ref: [Plestil. *J. J. Appl. Cryst.* **2000**, *33*, 600].

Capillary Zone Electrophoresis (CZE). For a smooth discussion, the experimental responses (electropherograms) were recalculated from a time domain into an electrophoretic mobility domain according the following Equation 3:

$$\mu_i^{\text{eff}} = \frac{l_{\text{UV}} l_{\text{tot}}}{U} \left(\frac{1}{t_{\text{EOF}}} - \frac{1}{t_i} \right) \quad (3)$$

where μ_i^{eff} is an electrophoretic mobility of the i -th compound, l_{UV} is an effective length of the capillary, l_{tot} is a total length of the capillary, U is a separation voltage, t_{EOF} is a migration time of EOF, and t_i is a migration time of the i -th compound.

Figures

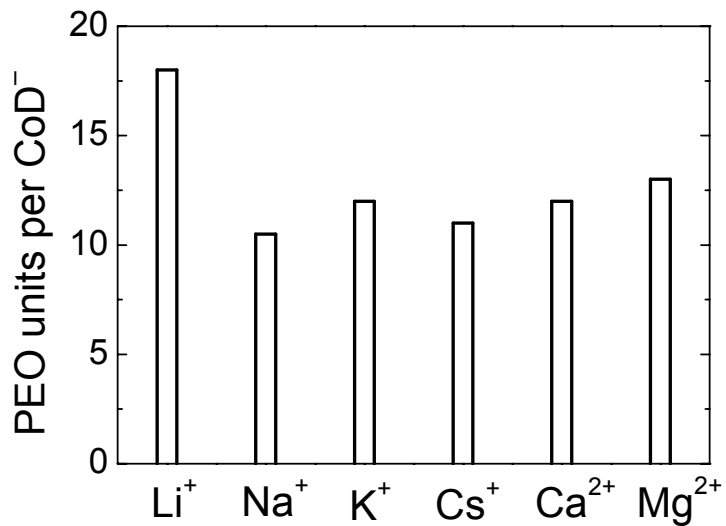


Fig. S1

Fig. S1 The number of overall PEO units per one complexed CoD^- anion in solutions of several alkali and earth-alkali cations of 0.1 M concentration.

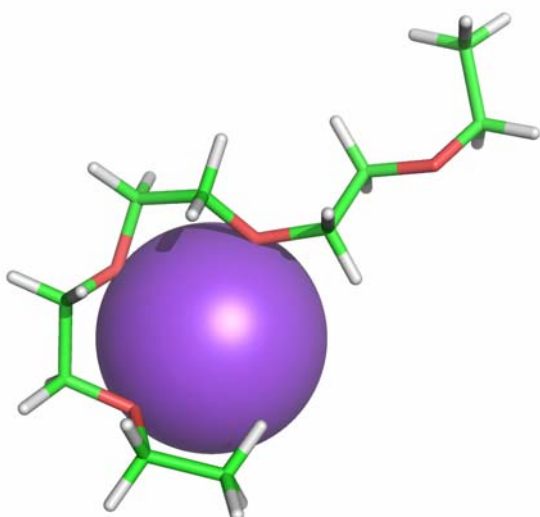


Fig. S2

Fig. S2 The optimized structure of the Na^+ and PEO-pentamer complex as a result of quantum mechanics calculations. Color-coding for EO_5 : green-carbon, red-oxygen, and white-hydrogen.

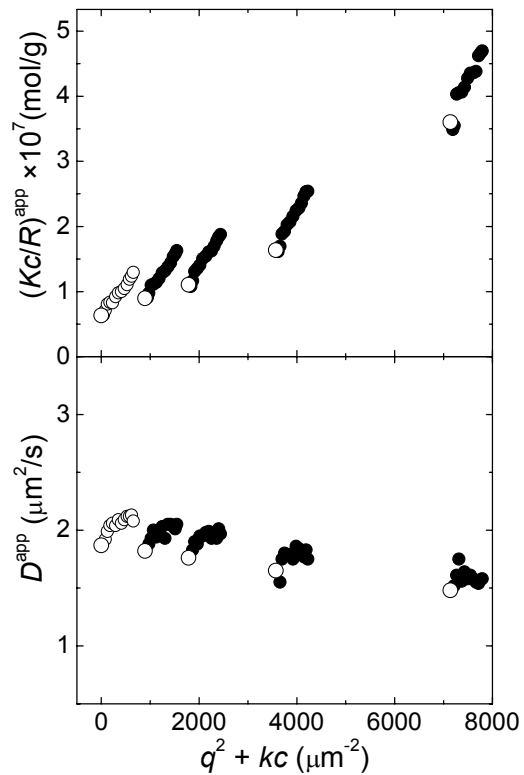


Fig. S3

Fig. S3 The static (top) and dynamic (bottom) Zimm plots of PMA-PEO/CoD⁻ particles in 0.05 M sodium tetraborate with the $\xi_{\text{PEO-CoD}}$ ratio 0.1.

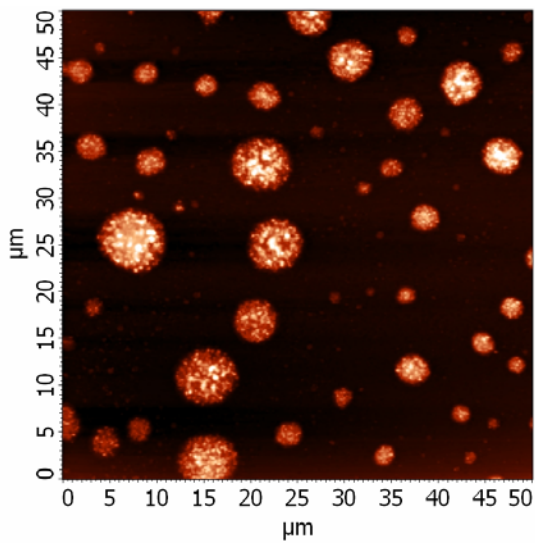


Fig. S4a

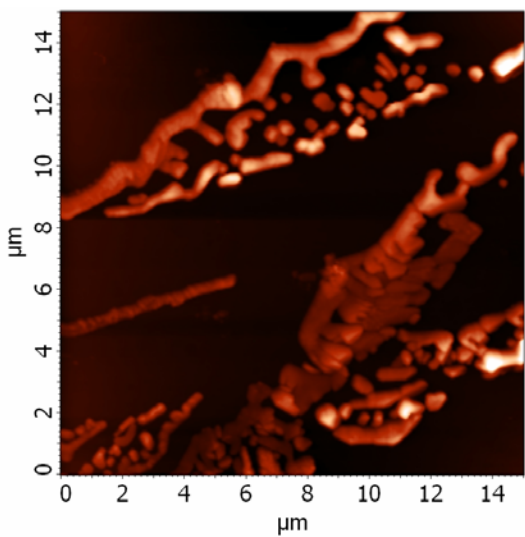


Fig. S4b

Fig. S4a,b The AFM scans of PMA-PEO/CoD⁻ particles with $\xi_{\text{PEO-CoD}}$ ratio 0.1 prepared by a deposition on mica from strongly acidic solution (corresponding to Figure 7).

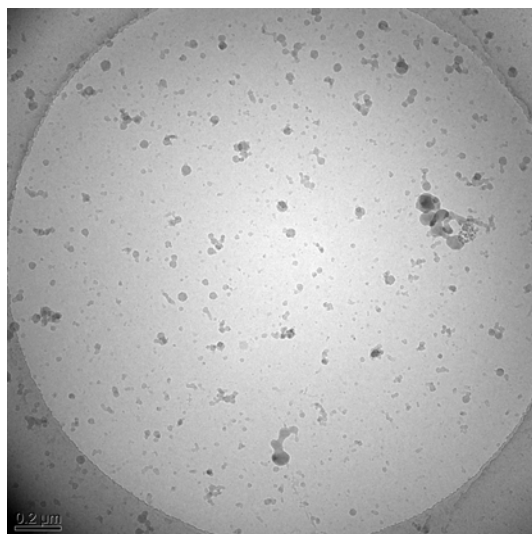


Fig. S4c

Fig. S4c The cryo-TEM micrograph of PMA-PEO/CoD⁻ particles with $\xi_{\text{PEO-CoD}}$ ratio 0.1 in strongly acidic solution (corresponding to Figure 8).

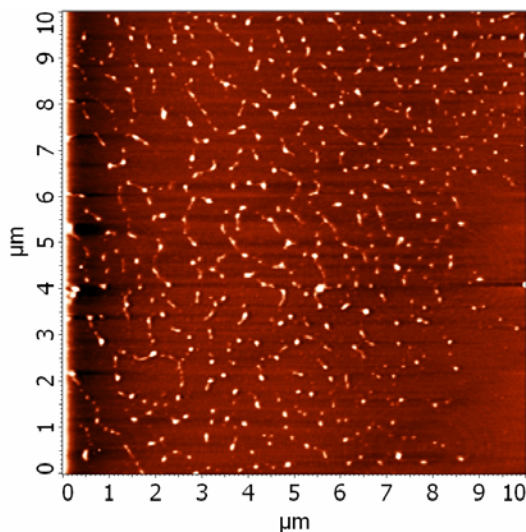


Fig. S4d

Fig. S4d The AFM scan of PMA-PEO/CoD⁻ particles with $\xi_{\text{PEO-CoD}}$ ratio 0.1 prepared by a slow titration and deposited on mica from basic solution.

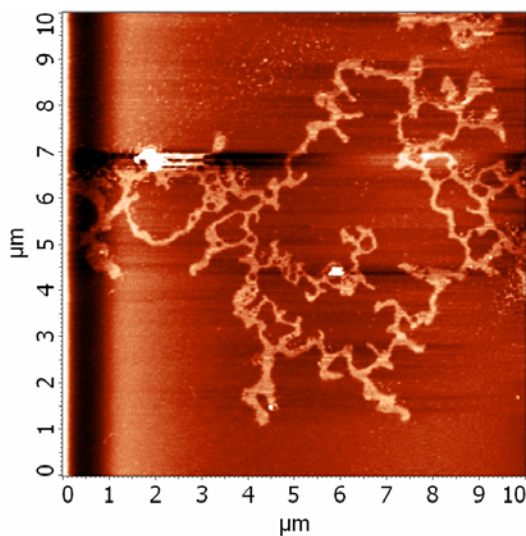


Fig. S4e

Fig. S4e The AFM scan of PMA-PEO/CoD⁻ particles with $\xi_{\text{PEO-CoD}}$ ratio 0.1 prepared by a slow titration and deposited on mica from strongly acidic solution.

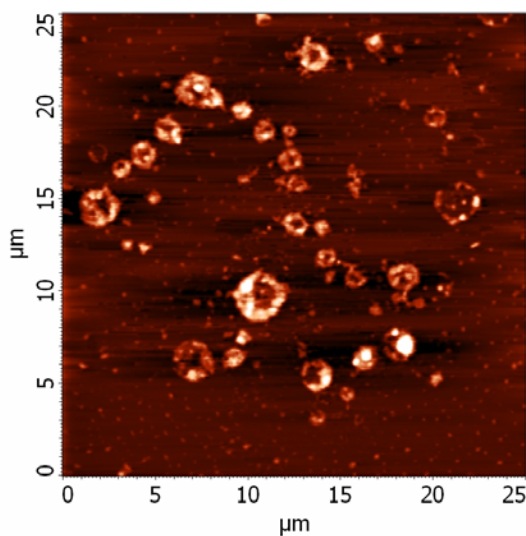


Fig. S4f

Fig. S4f The AFM scan of PMA-PEO/CoD⁻ particles with $\xi_{\text{PEO-CoD}}$ ratio 0.1 prepared by very slow dialysis and deposited on mica from basic solution.

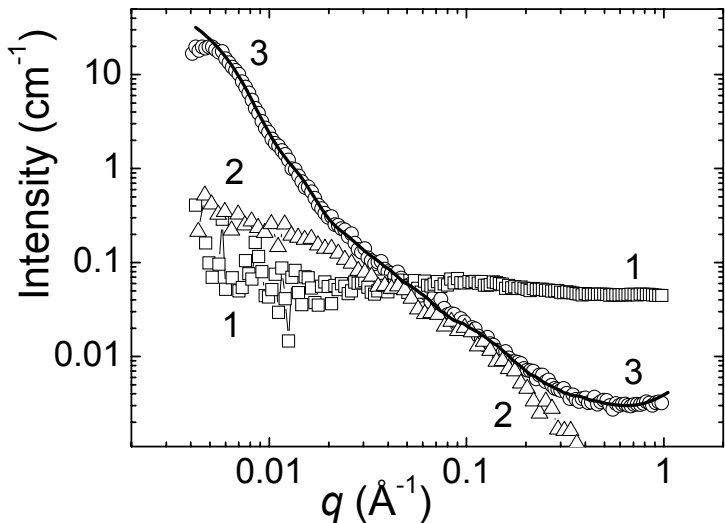


Fig. S5

Fig. S5 The SAXS curves of (1) NaCoD⁻ water solution ($c = 48$ g/L), (2) PEO-PMA solution in 0.05 M sodium tetraborate ($c = 5$ g/L), and (3) the PMA-PEO/CoD⁻ particles in 0.05 M sodium tetraborate with the $\xi_{\text{PEO-CoD}}$ ratio 0.1 ($c = 9.7$ g/L). The full line is a fit of curve 3 by the modified P&G model. (For details see corresponding text)

Comments on the fitting of SAXS data

The SAXS scattering curves for the nanoparticles (curve 3) and the parent samples (copolymer – curve 2, and metallacarborane – curves 1) are shown in Figure S5. The scattering curve 3 does not exhibit any features, which would allow us to use the bare-core approximation. The application of a more complex Pedersen & Gerstenberg model requires the knowledge of the scattering contrast values (Δb) of individual components (see Experimental section). Consistent results (shown in Table S1) were obtained only after two assumptions, one realistic and one auxiliary, had been made: (i) that the micellar cores are swollen by bulky CoD⁻ anions and (ii) that the system contains a non-negligible fraction of free chains. In this case, the SAXS results are comparable both with SLS and cryo-TEM data within experimental errors. The particle radius in Table S1 is slightly lower than the radius of gyration obtained by SLS (65 nm). The value of the core radius is ca. 19 nm. It is close to the dimensions of the dark stains in Figure 8. The copolymer aggregation number (ca. 97) as well as the value of M_w are significantly underestimated by SAXS, because the supplementary term corresponding to free PMA-PEO chains is unrealistically high (80 %). Because such a high fraction of free copolymer chains was

not detected by any of other experimental techniques used (NMR, SLS, AFM, and CZE), it suggests that the interpretation of the additional fitting term as a scattering from free copolymer chains is incorrect. A reasonable and significantly more probable explanation would be the following: The shape of curve 3 in Figure S5 reflects the scattering due to internal structure of aggregates and the supplementary term should be interpreted as a scattering contribution due to the inhomogeneity of nanoparticles.

Q_{core}	R_{core} (nm)	$R_{G,\text{chain}}$ (nm)	R_{particle} (nm)	n (cm ⁻³)	N_{agg}	M_w (g/mol)
8.6	18	18	54	1.3×10^{15}	97	9.3×10^6

Table S1 The SAXS characterization of the PMA-PEO/CoD⁻ particles by fitting Curve 3 in Figure S5 by the modified P&G Model (degree of core swelling Q_{core} , core radius R_{core} , radius of gyration of the shell-forming blocks $R_{G,\text{chain}}$, particle radius R_{particle} , number density n , weight average of copolymer aggregation number N_{agg} , weight average of particle molar mass M_w).

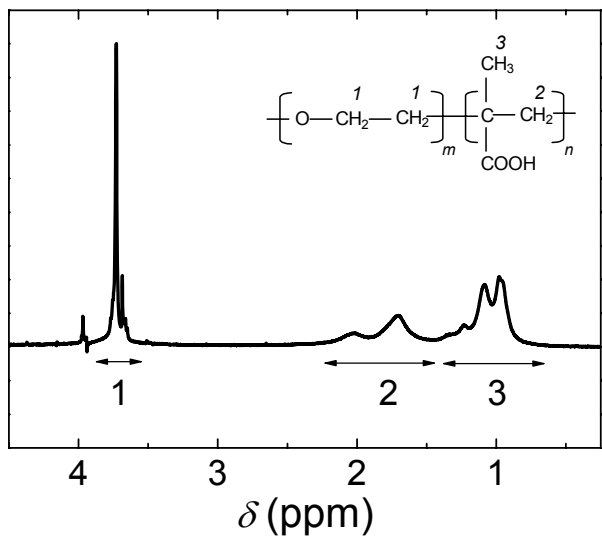


Fig. S6

Fig. S6 Typical ^1H NMR spectrum of PMA-PEO/CoD $^-$ particles in 0.05 M sodium tetraborate in D₂O. The numbers in the spectrum reflect the numbering of units in the schematics.

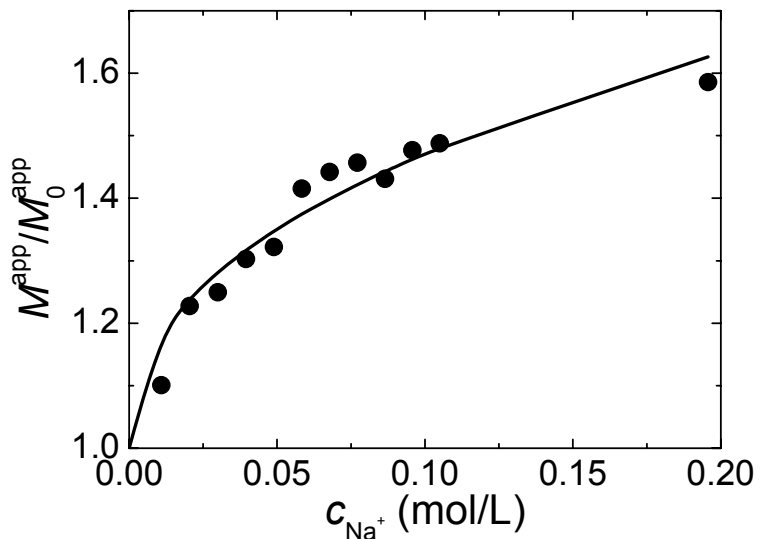


Fig. S7

Fig. S7 The relative molar mass of PMA-PEO/CoD $^-$ particles with $\xi_{\text{PEO-CoD}}$ ratio 0.1 in 0.005 M sodium tetraborate after addition of NaCl solution.